ELSEVIER

Polymer 43 (2002) 6931–6942

polymer

www.elsevier.com/locate/polymer

Influence of shear on polypropylene crystallization: morphology development and kinetics

Emmanuelle Koscher, René Fulchiron*

Laboratoire des Matériaux Polymères et des Biomatériaux, Bâtiment ISTIL, Universite Claude Bernard—Lyon1, 23, Boulevard du 11 Novembre 1918, 69622 Villeurbanne Cedex, France

Received 3 June 2002; received in revised form 29 August 2002; accepted 11 September 2002

Abstract

Crystallization experiments after shear treatment were performed to study the effect of shear on the crystallization kinetics and morphology of polypropylene. Experiments performed with a polarized light microscope revealed an increase in the number of activated nuclei after shear treatment, and alignment of these nuclei along flow lines after long shearing times. A crystallization half time was defined using the transmitted intensity between crossed polarizers, and rheological measurements. A kinetic model valid for PP crystallization under quiescent conditions was extended to include shear-induced crystallization by linking the extra number of activated nuclei observed after shear treatment to the first normal stress difference. This model accounts for the rheological behavior of the molten polymer and is then used to predict the higher sensitivity to shear treatment of long molecular weight fractions.

Keywords: Polypropylene; Crystallization; Shear treatment

1. Introduction

The microstructure formed during processing of polymer products determines the final properties such as dimensional accuracy, dimensional stability, thermal conductivity, modulus and strength. This explains the great interest (scientific as well as economic) in understanding flow induced crystallization, during which the microstructure of polymer products is formed according to the thermo-mechanical history of the polymer melt.

In order to study the relationship between thermo-mechanical history of polymer and the final microstructure and crystallization kinetics, polypropylene has many advantages and is frequently used by researchers. Indeed, its large-scale spherulitic structure enables crystallization to be observed with rheological measurements [1], as well as with optical experiments such as light diffraction [2,3] and microscopy [4–6], or with small [7,8] and wide-angle [9–12] X-ray diffraction.

Despite a consensus on the use of polypropylene as the most suitable polymer for flow-induced crystallization investigations, there is great variety in the method used to impose flow condition to the polymer melt. These methods can be divided into two categories: those which reproduce complex flow of one specific process [13,14], and which are then able to impose high levels of strain, and modified rheometers [1,15], or home-made devices [16–19] which generate better defined thermal and flow histories, but are unable to achieve conditions used in processing. The apparatus developed by Eder et al. [20] is an exception because it applies a well-defined flow history to the polymer melt, and uses an extruder-reservoir-die system to apply high strains. This device was improved by Kumaraswamy et al. [21] who reduced the size of polymer sample required for one experiment, and used X-ray diffraction to study the early stages of crystallization.

Although the range of shear strain applied varies significantly from one apparatus to another, the effect of shear on crystallization of polypropylene may be observed for very different flow conditions to those in commercial processing. Moreover, many authors have observed that during or after shear treatment, the crystallization process is dramatically accelerated; the number of activated nuclei is increased; and row nuclei or even shish-kebab structures are obtained for the highest levels of applied strain.

* Corresponding author. Tel.: +33-4-72-43-1567; fax: +33-4-78-89-2583.

E-mail address: rene.fulchiron@univ-lyon1.fr (R. Fulchiron).

0032-3861/02/$ - see front matter
PII: S0032-3861(02)00628-6

While the literature on flow-induced crystallization is large, only a few papers present both experimental results and models for the observed phenomena. The simplest models used to describe the enhancement of crystallization kinetics were built from the classical Avrami theory for crystallization of polymers in quiescent conditions, increasing the Avrami parameter n up to 6 or 7 [22] although usual theory predicts integer values between 1 and 3. These models are called continuum models. They include an orientation factor for the effect of flow [23], or directly modify the Avrami parameters with shear intensity [19]. Intermediate models also use the Avrami theory to describe the crystallization kinetics, but the nucleation or growth processes are modified by the effect of flow on the polymer melt thermodynamics [24,25]. More elaborate models are based on non-equilibrium thermodynamics [26,27]: in this, mass, momentum, and energy conservation equations are solved by taking into account both energy release due to the crystallization process and decrease of entropy in the polymer melt due to the flow. While the pressure effect on polymer crystallization can be described by its influence on the equilibrium melting temperature [28], the increase in the equilibrium melting temperature due to shear treatment calculated via the decrease of entropy, appears unrealistic [20]. This could be explained by the invalidity of the usual link between entropy and the equilibrium melting temperature under shear.

In the present work, the shear effect on the crystallization of polypropylene is studied from polarized light microscopy using a shearing hot stage and rheological experiments. A model is then developed to predict the crystallization kinetics. This model is based on the assumption that the rheological behavior of the polymer determines the sensitivity of the crystallization kinetics to the shear. Therefore, this sensitivity is implicitly linked to the molecular weight distribution of the polymer.

2. Experimental section

A commercial polypropylene (PP A) provided by Solvay was used for this study. The molecular weight ($M_w = 180.8 \times 10^3$ g/mol), and the polydispersity index ($M_w/M_n = 7.3$) were measured by Solvay using size exclusion chromatography.

2.1. Calorimetry experiments

Crystallization experiments were performed in a Perkin Elmer DSC 7 calorimeter. The calorimeter was first calibrated in temperature and heat flow. Slices of PP A pellets were placed in an aluminum sample pan and held at 210 °C for 5 min. The sample was then cooled down at the maximum cooling rate (−30 °C/min) to a temperature 10 °C higher than the crystallization temperature. The final 10° were cooled at a lower rate (−10 °C/min) in order to avoid over shoot below the crystallization temperature (Fig. 1).

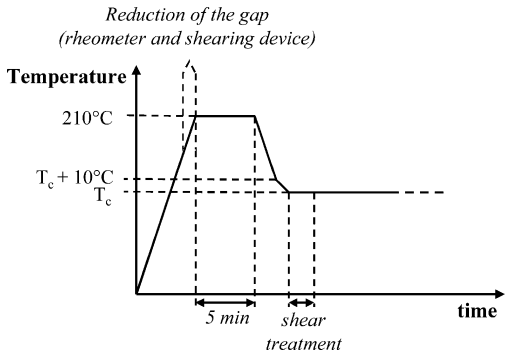

Fig. 1. Diagram of the temperature cycle.

During the crystallization process, the heat flow is recorded, and the relative crystallinity is calculated through the ratio of the crystallization peak area before time t over its total area. The half crystallization time $t_{1/2}$ is obtained for a relative crystallinity $\alpha = 0.5$.

2.2. Crystallization experiments under polarized microscope

In order to observe the crystallization process after short term shearing, a Leitz microscope was used in conjunction with a Linkam shearing hot stage (CSS 450 of Linkam Scientific Instruments, UK).

Polypropylene pellets were cut in half and inserted between the glass plates of the shearing device. The temperature was then increased to 210 °C. As soon as the pellets were molten ($T > 180$ °C), the upper plate was lowered to its final position $\delta = 0.15$ mm. After annealing at 210 °C for 5 min, the same cooling procedure as for calorimetry experiments was used to avoid over shoot below the crystallization temperature. The shear treatment was applied as soon as the isothermal condition was reached, and the data collection (pictures and/or transmitted intensity) started (Fig. 1). Three crystallization temperatures were investigated: 130, 134, and 140 °C. This range of crystallization temperatures allowed convenient experimental times both in quiescent condition and after shear treatment.

The intensity transmitted through the sample between crossed polarizers was recorded during the experiments. Fig. 2 presents examples of the curves obtained at 140 °C for a crystallization experiment in quiescent conditions and after shear treatment. There is no simple link between the crystallization state and the transmitted intensity. However, Fig. 2 shows a sigmoidal evolution for transmitted intensity versus time. Half crystallization times were estimated as

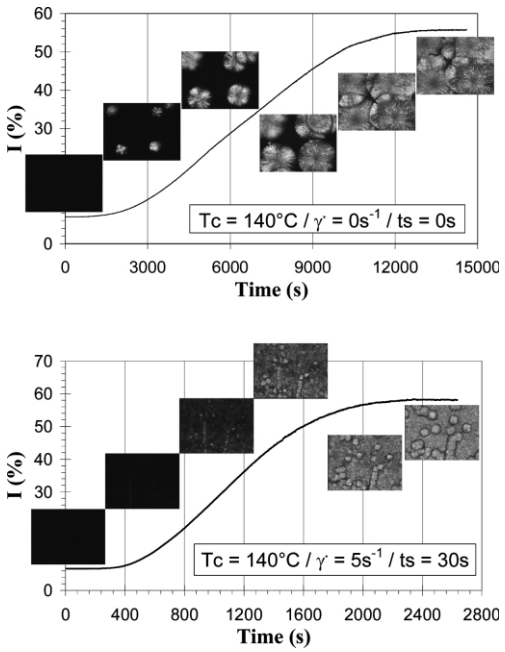

Fig. 2. Evolution of the transmitted intensity during crystallization process.

giving the intensity:

$$I(t_{1/2}) = \frac{I_{max} - I_{min}}{2} \quad (1)$$

2.3. Rheological experiments

Dynamic rheological experiments were performed for both relaxation spectrum extraction and crystallization monitoring. The rheometer was a Rheometrics RMS 800 used with the cone and plate configuration ($\phi = 25$ mm, cone angle = 0.1 rad).

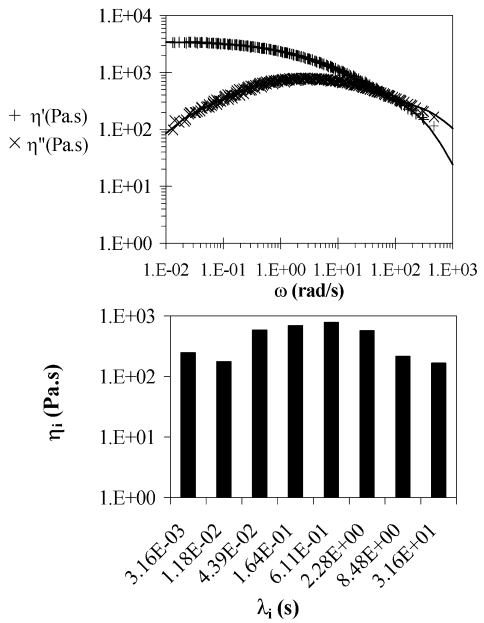

Fig. 3. Frequency sweep experiment and relaxation spectrum at $T = 203$ °C.

2.3.1. Frequency sweep experiments

In order to characterize the melt behavior of the polymer, dynamic frequency sweep experiments were performed at various temperatures. Then a master curve was built at 203 °C (Fig. 3) and, from an Arrhenius plot of the shift factors a_T, the activation energy was found to be $E_a = 45\ 080$ J/mol in agreement with literature data [29].

The master curve was then described using a N-mode Maxwell model [30]:

$$G'(\omega) = \sum_{i=1}^{N} \frac{G_i \omega^2 \lambda_i^2}{1 + \omega^2 \lambda_i^2} \qquad G''(\omega) = \sum_{i=1}^{N} \frac{G_i \omega \lambda_i}{1 + \omega^2 \lambda_i^2} \quad (2)$$

It is not the purpose of this paper to discuss the physical meaning of the relaxation spectrum used but it should be considered as a simple method to describe the linear viscoelastic behavior of the melt and provide data for the upper convected Maxwell model used later. Hence, eight relaxation times λ_i were chosen to cover the experimental frequency range. Their corresponding contributions G_i were then evaluated by minimizing

$$\sum_{j=1}^{M} (G'(\omega_j)/G'_j - 1)^2 + (G''(\omega_j)/G''_j - 1)^2$$

where M is the number of data points and G'_j and G''_j are the experimental values (Table 1).

2.3.2. Crystallization monitoring

Crystallization experiments in the rheometer cell were performed in order to validate the results obtained in microscopy with the shearing device. In these experiments, the crystallization process is monitored through the response of the sample to an oscillatory strain with a frequency $\omega = 1$ rad/s. At the start of crystallization, the sample is 'liquid' and a relative high strain has to be imposed to record a significant response. During crystallization, the sample becomes 'solid' and the imposed strain has to be lowered to remain in the linear domain. Indeed the imposed strain allows us to investigate the crystallization

Table 1
Relaxation spectrum for PP A at $T = 203$ °C

λ_i (s)	G_i (Pa)
3.162×10^{-3}	7.796×10^{4}
1.118×10^{-2}	1.489×10^{4}
4.394×10^{-2}	1.321×10^{4}
1.638×10^{-1}	4.202×10^{4}
6.105×10^{-1}	1.279×10^{4}
2.276	2.490×10^{2}
8.483	2.541×10^{1}
3.162×10^{1}	5.244

τ_n (s) $= 3.058 \times 10^{-2}$; τ_w (s) $= 2.626$; $\tau_w/\tau_n = 86$; G_n^0 (Pa) $= 8.98 \times 10^{4}$; η_0 (Pa s) $= 3.42 \times 10^{3}$.

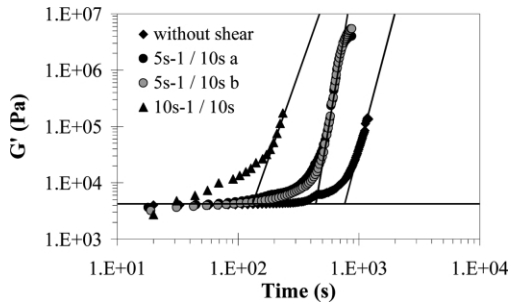

Fig. 4. $T_c = 134$ °C/isothermal crystallization experiments after shear treatment performed with the rheometer.

state of the sample, and it must not influence the crystallization kinetics or damage the crystallized sample. Practically, the strain was 20% at the beginning and 1% at the end.

In the rheometer, the polypropylene pellets were melted at 210 °C and held at this temperature for 5 min. The crystallization temperature was then reached as fast as possible (≈ -30 °C/min), and the shear treatment was programmed as a pre-shear option in the usual time sweep experiment.

Fig. 4 shows typical results of the measured G' versus time. Moreover, in this figure, two experimental curves for the same crystallization conditions are plotted (shear rate 5 s^{-1} for 10 s). Their similarity shows good reproducibility of the technique. Nevertheless, it should be mentioned that this technique is difficult because when solidifying, the sample shrinks and tends to detach from the cell plates before the experiment is complete. This was the case for two curves shown in Fig. 4 (without pre-shear and with a shear rate of 10 s^{-1}). Other difficulties could arise from the temperature control: indeed the rheometer sample is much larger than those used in the DSC and microscopy experiments, and the temperature control system was not designed to monitor precise crystallization experiments.

Despite these experimental difficulties, a crystallization time was defined at the intersection of the highest slope of the crystallization curve with the initial plateau.

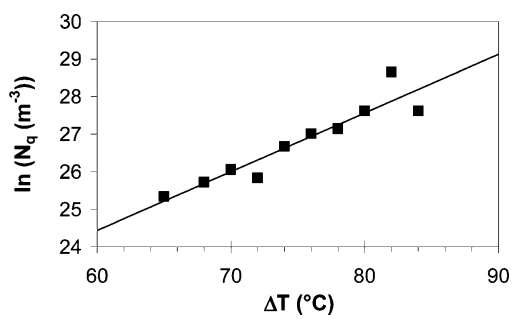

Fig. 5. Number of activated nuclei versus supercooling for crystallization experiments performed in quiescent conditions.

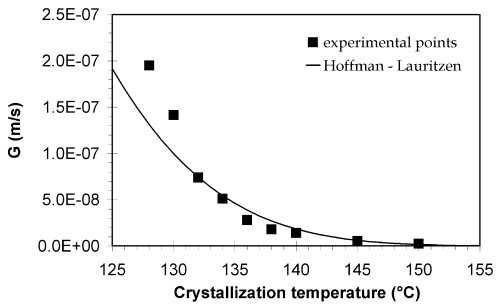

Fig. 6. Spherulite growth rate versus crystallization temperature.

3. Results and discussion

3.1. Crystallization in quiescent condition

3.1.1. $N_q(T)$ and $G(T)$

Experiments without shear treatment (quiescent condition) were performed under the microscope to evaluate the spherulite growth rate G by measuring the average spherulite diameter versus time and the number of activated nuclei N_q by numbering them on the pictures. Fig. 5 shows a linear variation of $\ln(N_q)$ with the supercooling ΔT (Eq. (3))

$$\ln(N_q) = a\Delta T + b \tag{3}$$

with $\Delta T = T_m^0 - T$, where T_m^0 is the equilibrium melting temperature which was taken equal to 210 °C [31]. This type of variation (Eq. (3)) was also observed by Kim [32], Binsbergen [33], and Angelloz [28]. In our case, $a = 1.56 \times 10^{-1}$ and $b = 1.51 \times 10^{1}$ (with N_q in m^{-3}) allow us to correctly describe the thermal dependence of the number of activated nuclei.

The Hoffman–Lauritzen theory [34] (Eq. (4)) was used to describe the variation of the spherulite growth rate with the temperature (Fig. 6)

$$G(T) = G_0 \exp\left(-\frac{U^*}{R(T - T_\infty)}\right)\exp\left(-\frac{K_g}{T\Delta T}\right) \tag{4}$$

Here, U^* is an energy parameter similar to an apparent activation energy of motion (often taken equal to 6270 J/mol for polypropylene [35]), R is the gas constant, and $T_\infty = T_g - 30$ °C is considered as the temperature at which no further molecular displacement is possible. The parameters $G_0 = 2.83 \times 10^2$ (m s^{-1}) and $K_g = 5.50 \times 10^5$ (K^2) were determined by plotting $\ln G + U^*/R(T - T_\infty)$ versus $(1/T\Delta T)$. As a result, their numerical value depends on U^*, T_∞, and T_m^0. Pospisil and Rybnikar determined a value for K_g in good agreement with the present value [31].

3.1.2. Kinetic model for crystallization in quiescent condition

In order to validate the equations established for $\ln N_q(\Delta T)$ and $G(T)$, the relative crystallinity $\alpha(t)$ was recalculated using the Avrami theory [36] (Eq. (5)) with a relationship between the Avrami constant K and the

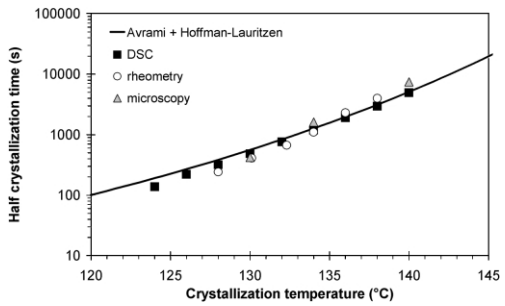

Fig. 7. Comparison between DSC, rheometry, and microscopy experimental values of half crystallization time and the values given by Avrami and Hoffman–Lauritzen theories using parameters determined with experiments performed under polarized microscope.

number of activated nuclei and growth rate given in Eq. (6)

$$\alpha(t) = 1 - \exp(-Kt^n) \text{ with } n = 3 \tag{5}$$

$$K = \tfrac{4}{3}\pi N_q G^3 \tag{6}$$

The half crystallization times calculated using Eqs. (4)–(6) are in good agreement with those obtained by DSC, rheometer and microscopy experiments (Fig. 7) over the whole range of temperatures studied (microscopy half crystallization time shown in Fig. 7 come from intensity recording). Therefore, it can be concluded that this kinetic model for crystallization in quiescent conditions is suitable. The whole approach of this model is summed up in Fig. 8. It can be pointed out that the parameters as well as their temperature dependence were defined only from crystallization experiments performed under polarized microscope.

This model was extended to non-isothermal conditions using the mathematical relationships between Nakamura [37], Ozawa [38] and Avrami theories (Eq. (7)). From the practical point of view, the logarithm of the Nakamura rate constant can be plotted against temperature (using Eqs. (3), (4), (6), and (7)) and fitted with a polynomial expression. Using this mathematical simplification, the kinetic model

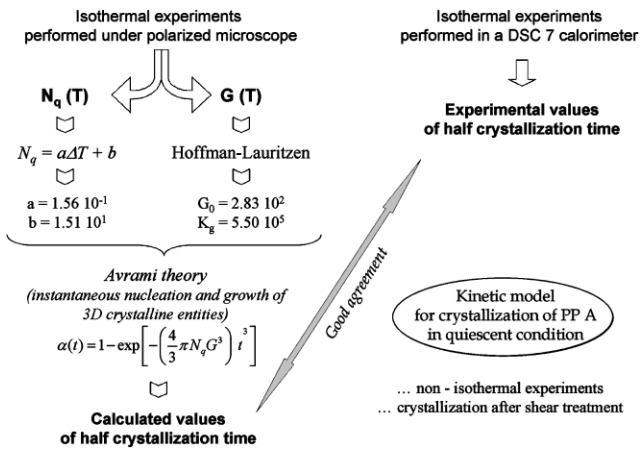

Fig. 8. Definition of a kinetic model for PP A crystallization in quiescent condition.

was able to describe non-isothermal crystallization experiments at both atmospheric pressure and high pressure by accounting for the effect of pressure on the equilibrium melting temperature [39]

$$\kappa_{\text{Nakamura}}(T) = K^{1/n}_{\text{Avrami}}(T)$$
$$\kappa_{\text{Nakamura}}(T) = -\frac{\mathrm{d}(k^{1/n}_{\text{Ozawa}}(T))}{\mathrm{d}T} \tag{7}$$

3.2. Shear effect

Fig. 9 shows the pictures taken during crystallization process after various shear treatments. Whatever the shear treatment applied, the crystallization process is enhanced compared to quiescent conditions and the crystallization time decreases as soon as a shear treatment is applied. The increasing number of activated nuclei is the first noticeable effect of an increasing shear rate. In the literature, the spherulite growth rate was also observed to increase under shear [19], but in this study the shear treatment is applied for a short time and the subsequent crystallization, which occurs in quiescent conditions, did not show any increase in the spherulite growth rate (Fig. 10).

After long shearing time, row nuclei can be observed. They form thread-like precursors before independent nuclei appear in the melt. This phenomenon was already observed by several groups [1,17,40–42], and more recently precisely characterized using WAXS and SAXS studies [2,7,11,43].

Before analyzing the results more deeply, one has to note the poor reproducibility of the crystallization experiments performed in the shearing device. The transmitted intensity, as well as the number of activated nuclei, depend strongly on the observation zone and should be representative of the whole sample. Unfortunately, no lens allowing a large observation was available and the results shown in Fig. 11 are averaged from several experiments performed at the same conditions and with the three techniques: DSC (without shear), microscopy, and rheometry (with and without shear).

Nevertheless, the equation chosen to estimate half crystallization time from recorded intensity (Eq. (1)) gave results in good agreement with those obtained by DSC when no shear treatment was applied (Fig. 7), and in good agreement with those obtained by rheometry after shear treatment (Fig. 11).

One can question if the glass windows of the shearing device promote nucleation leading to a transcrystalline layer which would hamper the measurement of the crystallization times and lead to overestimation. To investigate this, we performed some microscopic observations on cross-sections of samples crystallized either with or without shear treatment. However, no evidence of a transcrystalline layer has been demonstrated. Moreover, in the rheometer, the sample is so thick that a transcrystalline layer could not

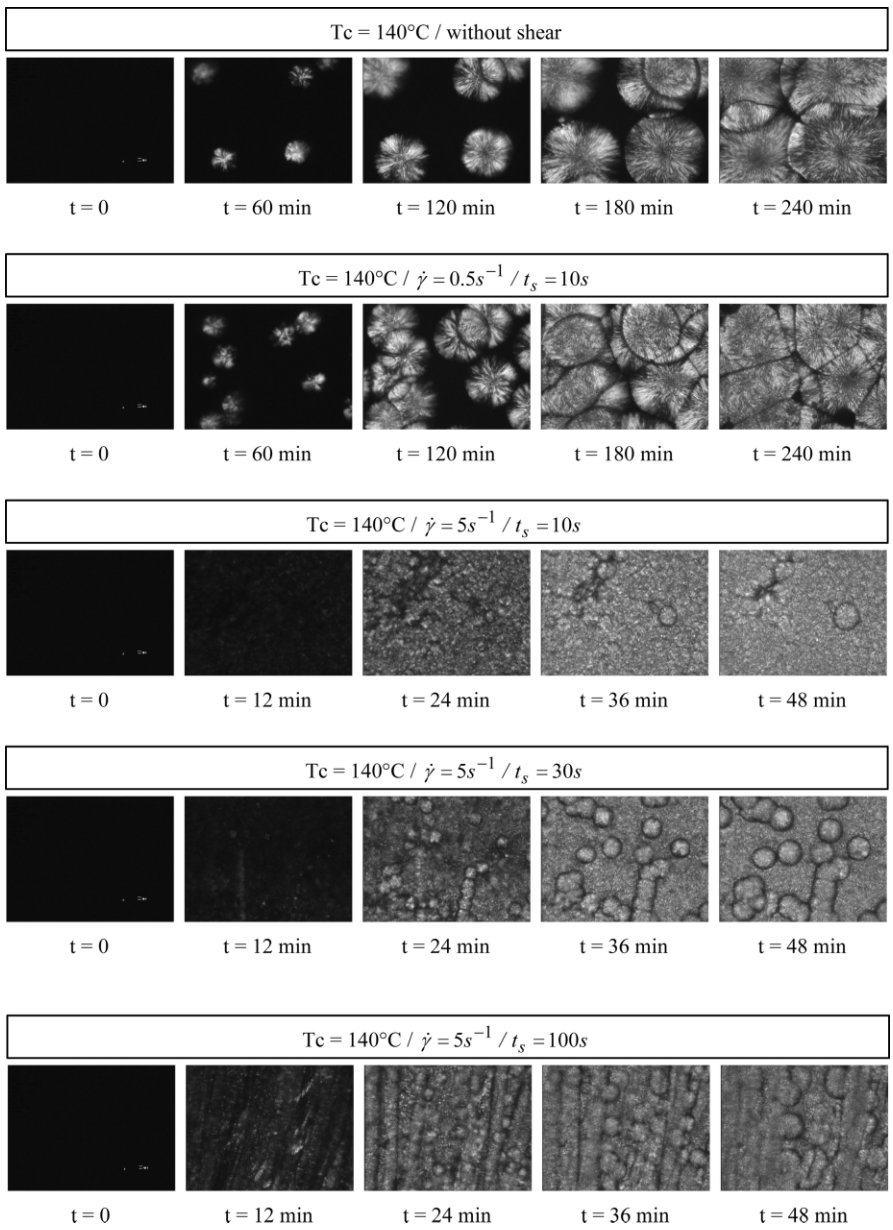

Fig. 9. Pictures taken during the crystallization process after various shear treatments (approximate pictures size: $470 \times 350\ \mu m^2$).

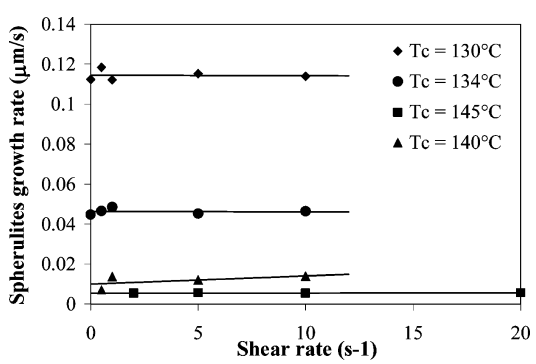

Fig. 10. Spherulite growth rate versus shear rate for different temperatures.

modify the measured crystallization time. Thus, the agreement between crystallization times obtained from rheometry and microscopy tends to corroborate the view that the results of microscopy are not affected by a transcrystalline layer.

3.3. Kinetic model

In order to predict crystallization kinetics after shear treatment, a model using Avrami theory and a shear modified number of activated nuclei was established. Such a model was inspired by Eder et al. [24] who expressed the number of activated nuclei N_0 as a function of $\dot{\gamma}^2$. Eder was then able to predict the thickness of thread like precursors. In the current study, the influence of shear on the number of

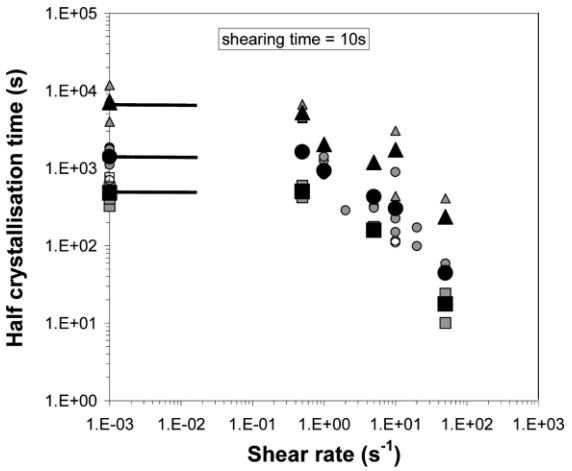

Fig. 11. Experimental half crystallization times versus shear rate. ▲: Shearing hot stage, $T_c = 140$ °C; ◍: shearing hot stage, $T_c = 134$ °C; ▨: shearing hot stage, $T_c = 130$ °C; ○: rheometer, $T_c = 134$ °C; □: rheometer, $T_c = 130$ °C; ▲: average values, $T_c = 140$ °C; ●: average values, $T_c = 134$ °C; ■: average values $T_c = 130$ °C. Horizontal lines show the average values at zero shear ($x = -\infty$ on a logarithmic scale) calculated from DSC, rheometry, and microscopy experiments (DSC results are not shown).

activated nuclei is incorporated in the usual Avrami theory assuming that the hypothesis of the theory is still valid after shear treatment. This means that the kinetic model will not be able to predict the formation of row nuclei or orientation in the sample, but will give an idea of the enhancement of the global kinetics due to the shear treatment.

Because of experimental observations (Fig. 9), the number of activated nuclei is written as the sum of the natural nuclei observed in quiescent condition N_q, and the nuclei appearing after shear treatment N_s (Eq. (8))

$$N = N_q + N_s \tag{8}$$

The number of activated nuclei in quiescent condition was evaluated from isothermal experiments (see Fig. 5 and Eq. (3)); the number of additional nuclei appearing after shear treatment was linked to the first normal stress difference N_1. This assumption can be justified by recalling that the first normal stress difference reflects the elastic part of the rheological behavior and hence the molecular orientation which can predispose some molecular segments to give a nucleus. Recently, Zuidema et al. [44] developed a comprehensive model where the nucleation rate enhancement was linearly linked to the second invariant of the volume invariant elastic Finger tensor which appears in the Leonov constitutive equation. Hence, the connection between the melt polymer elasticity and the sensitivity of the nucleation rate to the shear was accounted for. The present work follows a similar approach suitable to analyze our results despite some simplifying shortcuts. Other comments on the differences and similarities between their approach and the present model will be given later.

The simplest mathematical relationship between the additional number of activated nuclei appearing after shear treatment and the first normal stress difference N_1 is

$$\dot{N}_S = CN_1 \tag{9}$$

In quiescent conditions, the nucleation process is observed to be spontaneous, and the heterogeneous nuclei are probably the precursors of crystallization. The shear treatment may activate smaller heterogeneous nuclei, or homogeneous nuclei.

In his model, Eder links the number of primary and secondary activated nuclei to a function ϕ [20], which is a dimensionless variable describing the internal state of the melt, and which can be considered as the fraction of still existing entanglements. If the crystallization enhancement is due to the orientation of macromolecular chains in the sheared melt (lower entropy), the extra nucleation has to be linked to the viscoelastic behavior of the polymer. In the kinetic model presented here, the dimensionless variable ϕ is replaced by the first normal stress difference N_1 which is a representative measure of elasticity in the molten phase. As a consequence, the sensitivity of the polymer to the shear treatment depends directly on its relaxation time λ. This avoids introducing the parameter $\dot{\gamma}_a$ (critical shear rate of activation) used by Eder, yet the effect of the molecular weight distribution is implicitly taken into account by the model.

3.3.1. First normal stress difference calculation

In order to calculate the first normal stress difference, the stress tensor is expressed as a function of flow and polymer characteristics (Eq. (10)), in the framework of the upper convected Maxwell model [30]

$$\sigma = -p\mathbf{I} + \int_{-\infty}^{t} m(t-t')C_t^{-1}(t')\mathrm{d}t' \tag{10}$$

with p is the isotropic pressure; $\mathbf{I}$, the unit tensor; $m(t-t')$, the memory function of the polymer defined by $m(t) = -\mathrm{d}G(t)/\mathrm{d}t$, where $G(t)$ is the relaxation modulus and C_t^{-1} is the Finger relative strain tensor.

One can note that in the framework of the upper convected Maxwell model, the first normal stress difference is equivalent to the trace of the extra-stress tensor which Marruci links proportionally to the change of free energy due to shear treatment [45].

For a pure shearing flow, the Finger strain tensor is written as

$$C_t^{-1}(t') = \begin{bmatrix} 1+\gamma(t,t')^2 & \gamma(t,t') & 0 \\ \gamma(t,t') & 1 & 0 \\ 0 & 0 & 1 \end{bmatrix}$$

where $\gamma(t,t')$ is the total strain between times t' and t; and the

first normal stress difference is expressed as

$$N_1(t) = \int_{-\infty}^{t} m(t-t')\gamma^2(t,t')\mathrm{d}t' \tag{11}$$

where the memory function is written as

$$m(t) = -\frac{\mathrm{d}G(t)}{\mathrm{d}t} = \sum_i \frac{\eta_i}{\lambda_i^2}\exp\left(-\frac{t}{\lambda_i}\right) \tag{12}$$

with $\eta_i(=G_i\lambda_i)$ the viscous contribution associated to the λ_i relaxation time (Fig. 3). In improving Eder's kinetic model, Zuidema et al. [44] modified the rheological behavior of the polymer melt during the crystallization process. They argued that nucleation sites and crystalline regions can act as physical crosslinks and so increase the relaxation time and so flow-induced nucleation is a self-enhancing process.

In the present work, no effect of the crystalline part on the relaxation times were introduced, mainly because for most of the experiments, the shearing time was so short that the crystallinity was still very low when the shear was stopped. Therefore, the rheological behavior could be considered unaffected by the crystallinity. Nevertheless, the kinetic model was also applied to crystallization after long shearing time (same order of magnitude as the crystallization time) without relaxation time modification. Such modification could be an improvement to the model but, raises non-trivial questions about the relationship between λ and α [46,47].

For the shear treatment applied in this study ($\dot\gamma \neq 0$ for $t \in [0; t_S]$), the strain is written as:

$$\begin{aligned} t' < 0 &\Rightarrow \begin{cases} \gamma(t,t') = \dot\gamma t & \text{if } t \le t_S \\ \gamma(t,t') = \dot\gamma t_S & \text{if } t > t_S \end{cases} \\ t \in [0;t_S] &\Rightarrow \begin{cases} \gamma(t,t') = \dot\gamma\,(t-t') & \text{if } t \le t_S \\ \gamma(t,t') = \dot\gamma\,(t_S-t') & \text{if } t > t_S \end{cases} \\ t' > t_s &\Rightarrow \gamma(t,t') = 0 \end{aligned} \tag{13}$$

With the above equation, the first normal stress difference during and after shear treatment is expressed as

$$\text{if } t < t_s N_1(t) = 2\dot\gamma^2 \sum_i \lambda_i\eta_i\left[1-\left(1+\frac{t}{\lambda_i}\right)\exp\left(-\frac{t}{\lambda_i}\right)\right] \tag{14}$$

$$\text{if } t \ge t_s N_1(t) = 2\dot\gamma^2 \sum_i \lambda_i\eta_i\left[\exp\left(\frac{t_s}{\lambda_i}\right)-1-\frac{t_s}{\lambda_i}\right]\exp\left(-\frac{t}{\lambda_i}\right) \tag{15}$$

3.3.2. Relative crystallinity calculation

Using the Avrami kinetics model, the relative crystallinity can be written as $\alpha = 1-\exp(-\alpha')$, where α' is expressed as

$$\alpha'(t) = \int_0^t v(t,t')\dot N(t')\mathrm{d}t' \tag{16}$$

with $v(t,t')$ is the total volume at time t of a crystalline entity which started to grow at time t'. Note that spherulites impingement is taken into account by the relationship between α and α'.

Using Eq. (8), and considering that in quiescent conditions the activation frequency is very high for a very short time, Eq. (16) becomes

$$\alpha'(t) = \tfrac{4}{3}\pi G(T)^3\left[N_q t^3 + \int_0^t (t-t')^3\dot N_s(t')\mathrm{d}t'\right] \tag{17}$$

where $G(T)$ is the spherulite growth rate.

With Eq. (9), one obtains

$$\alpha'(t) = \tfrac{4}{3}\pi G(T)^3\left[N_q t^3 + C\int_0^t (t-t')^3 N_1(t')\mathrm{d}t'\right] \tag{18}$$

Finally, with Eqs. (14) and (15) of the first normal stress difference during and after shear treatment, α' is written as:

$$\begin{aligned} \alpha'(t) = \tfrac{4}{3}\pi G(T)^3\Bigg[N_q t^3 &+ 2\dot\gamma^2 C\sum_i \lambda_i\eta_i\int_0^{t_s}(t-t')^3 \\ &\times\left(1-\left(1+\frac{t'}{\lambda_i}\right)\exp\left(-\frac{t'}{\lambda_i}\right)\right)\mathrm{d}t' + 2\dot\gamma^2 C\sum_i \lambda_i\eta_i \\ &\times\left(\exp\left(\frac{t_S}{\lambda_i}\right)-1-\frac{t_S}{\lambda_i}\right)\int_{t_s}^{t}(t-t')^3\exp\left(-\frac{t'}{\lambda_i}\right)\mathrm{d}t'\Bigg] \end{aligned} \tag{19}$$

3.3.3. Half crystallization time calculation

The half crystallization time is obtained in Eq. (19) when $\alpha' = \ln(2)$ (Eq. 20)

$$\begin{aligned} \ln(2) = \tfrac{4}{3}\pi G(T)^3\Bigg[N_q t_{1/2}^3 &+ 2\dot\gamma^2 C\sum_i \lambda_i\eta_i\int_0^{t_s}(t_{1/2}-t')^3 \\ &\times\left(1-\left(1+\frac{t'}{\lambda_i}\right)\exp\left(-\frac{t'}{\lambda_i}\right)\right)\mathrm{d}t' + 2\dot\gamma^2 C\sum_i \\ &\times\lambda_i\eta_i\left(\exp\left(\frac{t_S}{\lambda_i}\right)-1-\frac{t_S}{\lambda_i}\right)\int_{t_s}^{t_{1/2}}(t_{1/2}-t')^3 \\ &\exp\left(-\frac{t'}{\lambda_i}\right)\mathrm{d}t'\Bigg] \end{aligned} \tag{20}$$

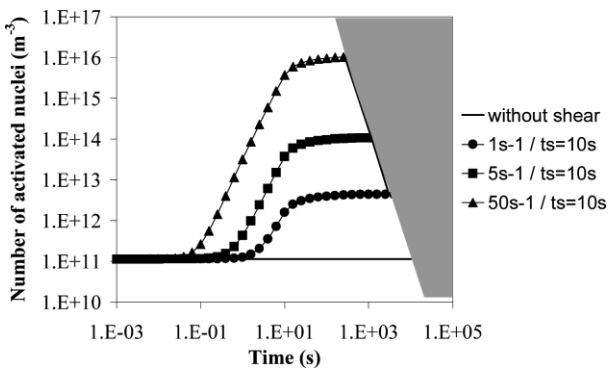

Fig. 12. $T_c = 140$ °C/calculated number of activated nuclei as a function of time for different shear rates.

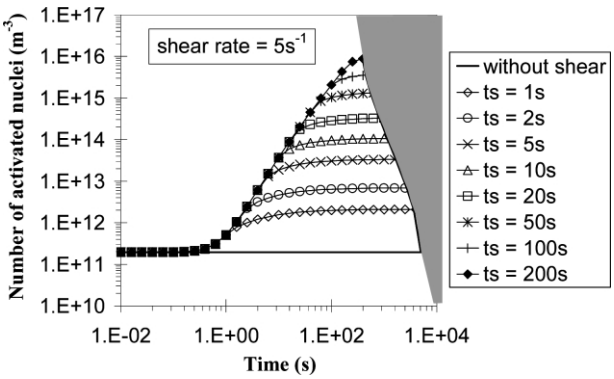

Fig. 13. $T_c = 140$ °C/calculated number of activated nuclei as a function of time for different shearing times.

Eq. (20) can be written analytically, but this form is not given here because of its size. A Newton–Raphson iterative method may be used to solve for $t_{1/2}$.

3.4. Kinetic model prediction

3.4.1. Polypropylene A

After shear treatment, the kinetic model (with $C = 10^6\ \mathrm{Pa}^{-1}\ \mathrm{s}^{-1}\ \mathrm{m}^{-3}$) predicts that the number of activated nuclei increases continuously to reach a value fixed by the shear intensity (Figs. 12 and 13). In Figs. 12 and 13, the graphs are limited by the crystallization zone giving the half crystallization time as a function of shear treatment. These half crystallization times were calculated with the kinetic model, and one can observe that for increasing shearing time the shear treatment tends to a limit because the theoretical half crystallization time becomes lower than the shearing time. For a shear rate of $5\ \mathrm{s}^{-1}$, this limit is $t_s = 200$ s (Fig. 13).

Looking at experimental results, it can be observed that the kinetic model predicts good trends for both the influence of shear rate (Fig. 14) and shearing time (Fig. 15). In Fig. 14, it can be noticed that the shear treatment becomes efficient for a decreasing shear rate when the shearing time increases. Actually, it becomes efficient when the number of nuclei activated by shearing becomes significantly higher than the natural nuclei number. This corresponds to departure from the lower plateau in Figs. 12 and 13. Hence, as mentioned

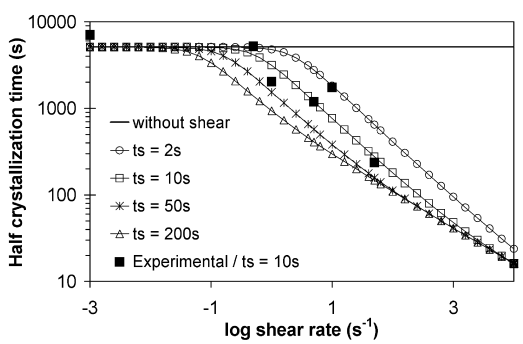

Fig. 14. $T_c = 140$ °C/experimental and calculated half crystallization time for different shearing times.

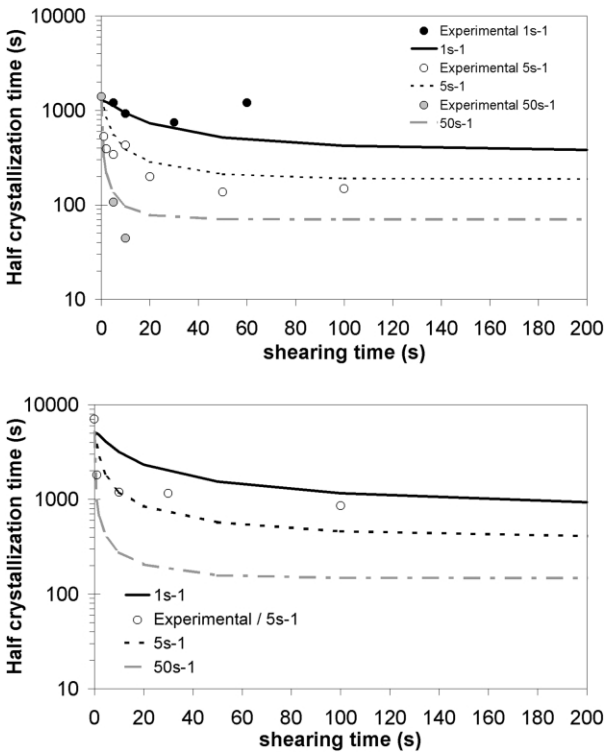

Fig. 15. Experimental and calculated half crystallization time versus shearing time for two crystallization temperatures and different shear rates/upper graph $T_c = 134$ °C/lower graph $T_c = 140$ °C.

earlier, the model can predict the critical shear rate $\dot{\gamma}_a$ of Eder.

The effect of temperature is taken into account through its influence on the spherulite growth rate and on the number of natural nuclei, but also through the ability of shear treatment to modify the nucleation process. Indeed, the expression of the first normal stress difference uses the relaxation times and the corresponding viscosities at the temperature considered. Nevertheless, the influence of temperature on the polymer viscosity is very low in the temperature range investigated compared to its influence on the spherulite growth rate and on the number of natural nuclei. Fig. 16 compares experimental and calculated values of the half crystallization time versus shear rate for the three crystallization temperatures investigated and a fixed

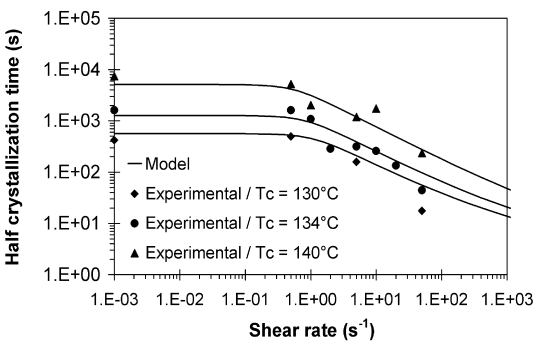

Fig. 16. Experimental and calculated half crystallization time versus shear rate for the three crystallization temperatures.

Table 2
Relaxation spectra for PP B, C, and D at 210 °C

λ_i (s)	G_i (Pa)		
	Polypropylene B; M_w (g mol^{-1}) = 231×10^3; $I_p = 2.7$	Polypropylene C; M_w (g mol^{-1}) = 235×10^3; $I_p = 7$	Polypropylene D; M_w (g mol^{-1}) = 374.5×10^3; $I_p = 9$–10
10^{-2}	6.2	5.009	4.021
3.728×10^{-2}	1.465×10^1	1.319×10^1	1.71×10^1
1.389×10^{-1}	1.519×10^2	1.695×10^2	2.486×10^2
5.179×10^{-1}	2.94×10^2	6.437×10^2	1.506×10^3
1.931	1.365×10^3	2.773×10^3	9.685×10^3
7.197	7.736×10^2	6.179×10^3	3.617×10^4
2.683×10^1	2.954×10^3	1.568×10^4	1.325×10^5
10^2	2.675×10^3	2.127×10^4	2.821×10^5

Polypropylene B: τ_n (s) = 4.427×10^{-2}; τ_w (s) = 2.272; $\tau_w/\tau_n = 51$; G_n^0 (Pa) = 8.189×10^4; η_0 (Pa s) = 3.625×10^3. Polypropylene C: τ_n (s) = 8.946×10^{-2}; τ_w (s) = 7.291; $\tau_w/\tau_n = 81$; G_n^0 (Pa) = 7.165×10^4; η_0 (Pa s) = 6.409×10^3. Polypropylene D: τ_n (s) = 3.135×10^{-1}; τ_w (s) = 1.979×10^1; $\tau_w/\tau_n = 63$; G_n^0 (Pa) = 7.452×10^4; η_0 (Pa s) = 2.336×10^4.

shearing time of 10 s. Again, the model predictions are very close to the experimental data. It must be pointed out that the same value of scale factor C (10^{-6} Pa^{-1} s^{-1} m^{-3}) was used for all these calculations. Therefore, this parameter seems to be independent of the temperature, which was not obvious a priori. Hence, it can be concluded that the model explicitly accounts for all the temperature effects.

3.4.2. Extension of kinetic model prediction

One of the advantages of the kinetic model is its ability to take into account the polymer melt rheological behavior. It was used to predict the crystallization kinetics of three other polypropylenes after shear treatment. These polymers are labeled B, C, and D, and their characteristics are presented in Table 2. They all have a molecular mass higher than polypropylene A. Both of them have an intermediate molecular mass and two different polydispersities (metallocene polymerized narrow molecular weight distribution: polypropylene B; Ziegler–Natta polymerized broad molecular weight distribution: polypropylene C). The last one (Ziegler–Natta polymerized polypropylene D) has the highest molecular mass and a broad molecular weight distribution.

The rheological melt behavior of these polypropylenes was investigated using frequency sweep experiments

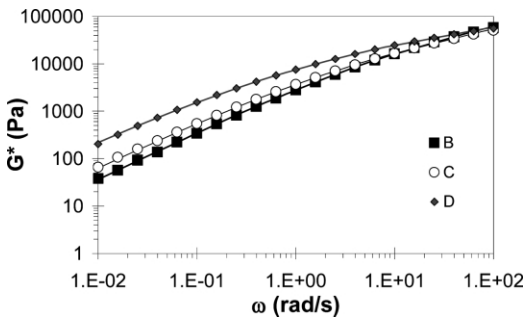

Fig. 17. Frequency sweep experiments at 210 °C for polypropylenes B, C, and D.

performed at 210 °C. As for polypropylene A, the relaxation times λ_i and their corresponding moduli G_i used in Eq. (2) were adjusted on G', and G'' curves (see Fig. 17 and Table 2).

The isothermal experiments after shear treatment were performed with the rheometer at two different temperatures. Indeed, from Hoffman–Weeks analyses, a preliminary study showed that the equilibrium melting temperature of the metallocene polypropylene (B) was 10 °C lower than those of the Ziegler–Natta materials (C and D) [48]. This difference was attributed to a higher head-to-head defect amount in metallocene polypropylene. The isothermal crystallization experiments were performed at a same supercooling, which means at 135 °C for the polypropylene B, and at 145 °C for the polypropylenes C and D.

Some crystallization experiments were performed under the polarized microscope in order to determine the number of activated nuclei and the spherulite growth rate of the three polypropylenes in quiescent condition. Since these experiments were performed at only one temperature, the variations of N_0 and G with the temperature were not established for polymers B, C and D, so experimental values were directly introduced in the kinetic model. It should be noted that no increase of the spherulite growth rate was observed after shear treatment even for the highest molecular weight polypropylene D.

As for polypropylene A, the numbers of activated nuclei determined on the pictures and the experimental spherulite

Table 3
Half crystallization times (rheological experiments) after shear treatment

	Polypropylene		
	B	C	D
Without shear	8580	9240	15 000
$\gamma = 5$ s^{-1}/$t_s = 10$ s	4740	6240	1020
$\gamma = 10$ s^{-1}/$t_s = 10$ s	2250	1980	660

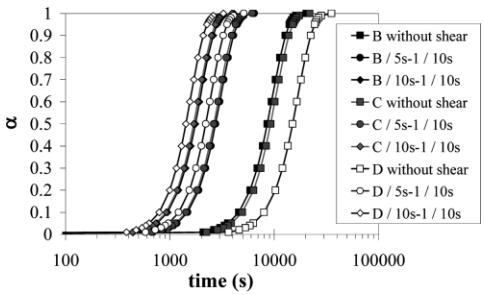

Fig. 18. Calculated relative crystallinity as a function of time.

growth rates give, using Avrami theory (Eqs. (5) and (6)), half crystallization times in good agreement with those measured by rheometry when no shear treatment is applied (which validates the first experiments performed with both techniques).

As hoped, the calculations using the kinetic model describe well (at least qualitatively) the experimental observations: Table 3 shows the experimental half crystallization times obtained by rheometry, and Fig. 18 shows the calculated relative crystallinity. Note that these calculations were performed by introducing different values of α' in Eq. (19) and solving the equation for the corresponding times (not only $t_{1/2}$ as in Eq. (20)). Here again, the scale factor C was the same for all calculations. In quiescent condition the highest molecular mass polypropylene (D) crystallizes slower than the two other ones, but because of its long macromolecules it is much more sensitive to the shear treatment and it crystallizes faster than the two other ones as soon as a shear treatment is applied.

On the other hand, polypropylenes B and C crystallize more or less in the same time in quiescent condition or after shear treatment. This suggests that the effect of shear is more sensitive to the average molecular weight than to the polydispersity index.

3.4.3. Additional comments

In its present form, the model deals with the effect of shear on the crystallization kinetics but it does not attempt to describe the final morphology. In other words, the appearance of shish kebabs or thread-like nuclei is not predicted as in the more sophisticated model of Zuidema et al. [44]. It should be noted that this sophistication requires more adjustable parameters whereas in our work, only one parameter was used to link the nucleation rate to the melt polymer elasticity.

One of the main issues of this work is that the critical shear rate $\dot{\gamma}_a$ from which the crystallization time becomes shear rate dependent is a result of the modeling. This critical shear rate is reached when the supplementary nucleation due to the shear becomes more important than the natural nucleation. Moreover, the shear nucleation enhancement is controlled by the viscoelastic behavior of the polymer contrary to the natural nucleation. Hence, for example, it can be presumed that incorporating a nucleating agent in a polymer will increase the natural nuclei number so that the critical shear rate would be shifted to higher values.

Additionally, various improvements to the model presented should be investigated. For example, the rheological behavior has been described using the upper convected Maxwell model. This choice was led by the relative simplicity of calculations. More complex models such as Wagner or Phan–Thien–Tanner models [30] may be used for a more accurate description of the melt behavior if necessary. Nevertheless, the fact that the first normal stress difference is generally overpredicted by the upper convected Maxwell model can be counterbalanced by the scale factor C in Eq. (9). Another questionable point should be the use of a simple linear link between the first normal stress difference N_1 and the nucleation rate due to the shear $\dot{N}_s$. Indeed, one can suppose that the relationship between these two functions could be more complex and that the introduction of different nucleation types could lead to a description of the final morphology [44].

4. Conclusion

In this study, crystallization experiments performed after shear treatment under polarized microscope, as well as with a rheometer, allowed us to quantify the enhanced crystallization kinetics. A kinetic model established for crystallization in quiescent condition was extended to crystallization after shear treatment by linking the extra number of activated nuclei to the first normal stress difference. This model has the advantage of taking into account the polymer melt rheological behavior through the first normal stress difference calculation. It is able to qualitatively predict the sensitivity of three polypropylenes with different molecular weight distributions to the shear treatment and could be improved by further experiments on other polypropylenes.

Acknowledgements

We want to acknowledge gratefully the companies Legrand, Solvay, and Moldflow for the supply of material, material characterization and for financial support. We would like to thank more particularly Peter Kennedy, Rong Zheng, Vito Leo, Luc Dheur, Jean-Michel Rossignol, Michel Laplanche Gilles Régnier, Géraldine Poutot and Didier Delaunay for stimulating discussions. Crystallization experiments on polypropylenes B, C, and D were performed with the help of Sofian Berra.

References

[1] Pogodina NV, Winter HH, Srinivas S. J Polym Sci. Part B. Polym Phys 1999;37:3512–9.
[2] Kumaraswamy G, Issaian AM, Kornfield JA. Macromolecules 1999; 32:7537–47.
[3] Pogodina NV, Lavrenko VP, Srinivas S, Winter HH. Polymer 2001; 42(21):9031–43.
[4] Duplay C, Monasse B, Haudin JM, Costa JL. Polym Int 1999;48: 320–6.
[5] Jay F, Haudin JM, Monasse B. J Mater Sci 1999;34:2089–102.
[6] Liedauer S, Eder G, Janeschitz-Kriegl H, Jerschow P, Geymayer W, Ingolic E. Int Polym Proces VIII 1993;3:236–44.
[7] Somani RH, Hsiao BS, Nogales A, Srinivas S, Tsou AH, Sics I, Balta-Calleja FJ, Ezquerra TA. Macromolecules 2000;33:9385–94.
[8] Nogales A, Hsiao BS, Somani RH, Srinivas S, Tsou AH, Balta-Calleja FJ, Ezquerra TA. Polymer 2001;42(12):5247–56.
[9] Moitzi J, Skalicky P. Polymer 1993;34(15):3168–72.
[10] Pople JA, Mitchell GR, Chai CK. Polymer 1996;37(18):4187–91.
[11] Pople JA, Mitchell GR, Sutton SJ, Vaughan AS, Chai CK. Polymer 1999;40(10):2769–77.
[12] Göschel U, Swartjes FHM, Peters GWM, Meijer HEH. Polymer 2000; 41(4):1541–50.
[13] Janarthanan R, Garg SN, Misra A. J Appl Polym Sci 1994;1:1175–82.
[14] Xie B, Bigio DI. ANTEC'95 1995;389–93.
[15] Kobayashi K, Nagasawa T. J Macromol Sci—Phys 1970;B4:331–45.
[16] Lagasse RR, Maxwell B. Polym Engng Sci 1976;16:189–99.
[17] Fritzsche AK, Price FP, Ulrich RD. Polym Engng Sci 1976;16:182–8.
[18] Monasse B. J Mater Sci 1992;27:6047–52.
[19] Monasse B. J Mater Sci 1995;30:5002–12.
[20] Eder G, Janeschitz-Kriegl H, Liedauer S. Prog Polym Sci 1990;15: 629–714.
[21] Kumaraswamy G, Verma RK, Kornfield JA. Rev Sci Instrum 1999; 70:2097–104.
[22] Sherwood CH, Price FP, Stein RS. J Polym Sci: Polym Symp 1978;63: 77–94.
[23] Michaeli W, Keller H. Comput Mater Sci 1996;7:253–6.
[24] Eder G, Janeschitz-Kriegl H, Krobath G. Prog Colloid Polym Sci 1989;80:1–7.
[25] Coppola S, Grizzuti N, Maffettone PL. Macromolecules 2001;34: 5030–6.
[26] Bushman AC, McHugh AJ. J Polym Sci. Part B. Polym Phys 1996;34: 2393–407.
[27] Poitou A, Ammar A. Compte Rendu de l'Académie des Sciences 2001;329:5–11.
[28] Angelloz C, Fulchiron R, Douillard A, Chabert B, Fillit R, Vautrin A, David L. Macromolecules 2000;33:4138–45.
[29] Gahleitner M. Prog Polym Sci 2001;26:895–944.
[30] Bird RB, Armstrong RC, Hassager O. Dynamics of polymeric liquids, 2nd ed. Fluid mechanics, vol. 1. New York: Wiley; 1987.
[31] Pospisil L, Rybnikar F. Polymer 1990;31(3):476–80.
[32] Kim CY, Kim YC, Kim SC. Polym Engng Sci 1993;33:1445–51.
[33] Binsbergen FL, De Lange BGM. Polymer 1970;11(6):309–26.
[34] Hoffman JD, Miller RL. Polymer 1997;38(13):3151–212.
[35] Hoffman JD, De Lange BGM, Lauritzen JIJ. In: Hannay NB, editor. Treatise on solid state chemistry, vol. 3. New York: Plenum Press; 1976. chapter 7.
[36] Avrami M. J Chem Phys 1939;7:1103–12.
[37] Nakamura K, Watanabe K, Katayama K, Amano T. J Appl Polym Sci 1972;16:1077–91.
[38] Ozawa T. Polymer 1971;12(3):150–8.
[39] Fulchiron R, Koscher E, Poutot G, Delaunay D, Regnier G. J Macromol Sci—Phys 2001;B40:297–314.
[40] Larsen A, Hande O. Colloid Polym Sci 1993;271:277–89.
[41] Hosier IL, Bassett DC, Moneva IT. Polymer 1995;36(22):4197–202.
[42] Jerschow P, Janeschitz-Kriegl H. Rheol Acta 1996;35:127–33.
[43] Kumaraswamy G, Verma RK, Issaian AM, Wang P, Kornfield JA, Yeh F, Hsiao BS, Olley RH. Polymer 2000;41(25):8931–40.
[44] Zuidema H, Peters GWM, Meijer HEH. Macromol Theory Simul 2001;10:447–60.
[45] Marrucci G. Trans Soc Rheol 1972;16:321–30.
[46] Boutahar K, Carrot C, Guillet J. Macromolecules 1998;31:1921–9.
[47] Pogodina NV, Winter HH. Macromolecules 1998;31:8164–72.
[48] Duplay C. Influence de la structure moléculaire sur la cinétique de cristallisation de polypropylenes en écoulement de cisaillement. PhD Thesis. Ecole des Mines de Paris, Sophia-Antipolis, France; 2001.